instruments

MDPI

Boron Nitride Nanotube Cyclotron Targets for Recoil Escape Production of Carbon-11

Johanna Peeples [1],*, Sang-Hyon Chu [2], James P. O'Neil [3], Mustafa Janabi [3], Bruce Wieland [1] and Matthew Stokely [1]

[1] BTI Targetry LLC, 1939 Evans Road, Cary, NC 27513, USA; wielandb@bellsouth.net (B.W.);
     stokely@btitargetry.com (M.S.)
[2] National Institute of Aerospace, 100 Exploration Way, Hampton, VA 23666, USA; schu@nianet.org
[3] Lawrence Berkeley National Laboratory, 1 Cyclotron Road, Berkeley, CA 94720, USA;
     jponeil@lbl.gov (J.P.O.); mjanabi@lbl.gov (M.J.)
*   Correspondence: peeples@btitargetry.com; Tel.: +1-919-677-9799

check for
updates

Abstract: Boron nitride nanotubes (BNNTs) were investigated as a target media for cyclotron production of ^{11}C for incident beam energy at or below 11 MeV. Both the $^{11}B(p,n)^{11}C$ and $^{14}N(p,\alpha)^{11}C$ nuclear reactions were utilized. A sweep gas of nitrogen or helium was used to collect recoil escape atoms with a desired form of $^{11}CO_2$. Three prototype targets were tested using an RDS-111 cyclotron. Target geometry and density were shown to impact the saturation yield of ^{11}C and percent of yield recovered as carbon dioxide. Physical damage to the BNNT target media was observed at beam currents above 5 μA. Additional studies are needed to identify operating conditions suitable for commercial application of the method.

Keywords: cyclotron target; carbon-11; recoil escape; boron nitride nanotubes; BNNTs

1. Introduction

Boron nitride nanotube (BNNT) nanomaterials [1–5] can be used in a recoil escape target to produce ^{11}C for incident proton energy at or below 11 MeV. This would enable ^{11}C production for economical low-energy cyclotrons [6–9], and it could be used to increase production from conventional ^{11}C gas targets on MiniTrace and RDS-111 cyclotrons. Preliminary experiments have demonstrated recoil escape production and recovery of small quantities of $^{11}CO_2$, and there has been a continued effort to develop a target design and platform that can be used to produce viable yields for a commercial system.

Conventional gas targets for ^{11}C production operate by proton bombardment of nitrogen gas [10–13]. However, due to the low nuclear cross-section of the $^{14}N(p,\alpha)^{11}C$ nuclear reaction below 11 MeV, this production method is not commercially viable for accelerators with proton energy in the range of 7–10 MeV. Adding BNNT nanomaterials to the target allows for an additional production route via the $^{11}B(p,n)^{11}C$ nuclear reaction, which has a higher cross-section at all proton energies, as shown in Figure 1 [14,15]. If the produced ^{11}C can be effectively recovered from the target, the total yield of ^{11}C will be greater than currently achievable using a conventional gas target.

The nanotube geometry should offer superior recovery of ^{11}C recoil atoms to boron powder, due to the smaller mean particle size (nm versus μm) and higher porosity. Nearly complete recoil escape should be possible, because the walls of individual BNNT fibrils are single atomic thickness or at most a few atoms thick. The high porosity of the bulk material should allow sufficient gas flow to facilitate the slowing of recoil ions to thermal energies and their combination with trace oxygen in the sweep gas.
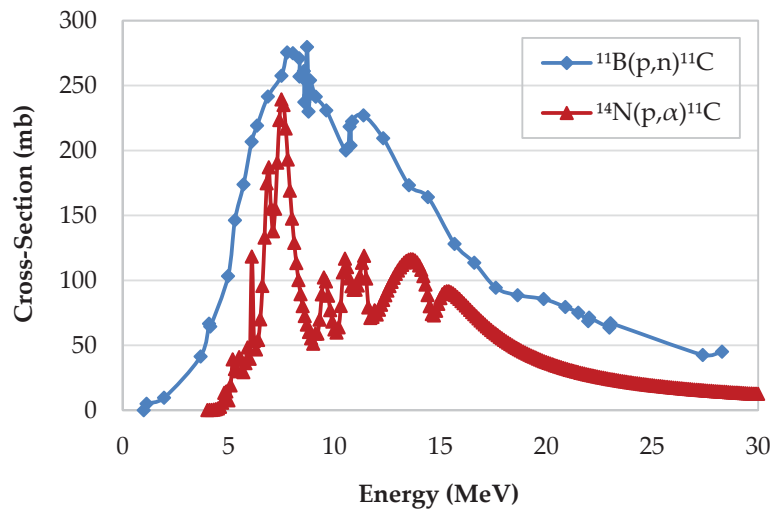
Figure 1. Cross-sections for ^{11}C production from the ^{11}B(p,n)^{11}C and ^{14}N(p,α)^{11}C nuclear reactions.

2. Materials and Methods

Both natural-abundance boron (19.9% ^{10}B and 80.1% ^{11}B) and enriched boron-11 (>98% ^{11}B) BNNT nanomaterials are commercially available [16]. The bulk material is highly porous, allowing for diffusion of gas, and the nanotube dimensions are compatible with the recoil escape of ^{11}C. In addition to the nanotubes, impurities of elemental boron and hexagonal boron nitride (*h*-BN) are present. Recovery of ^{11}C is assumed to be strongly correlated to the impurity content, since larger structures could trap recoiling atoms and prevent recovery in the sweep gas. The BNNT material is supplied at a low density of roughly 1.38 g/cm^3 [17]. It undergoes plastic deformation with light pressure and sticks to surfaces both mechanically and due to electrostatic attraction. As a result, loading a target at uniform density is challenging. A photograph of the bulk BNNT material is shown in Figure 2, and individual nanotubes and nontube impurities, such as boron and *h*-BN particles, can be seen in the scanning electron microscope (SEM) images shown in Figure 3.

Figure 2. Photograph of 500-mg sample of bulk boron nitride nanotube (BNNT) material from BNNT, LLC, supplier.
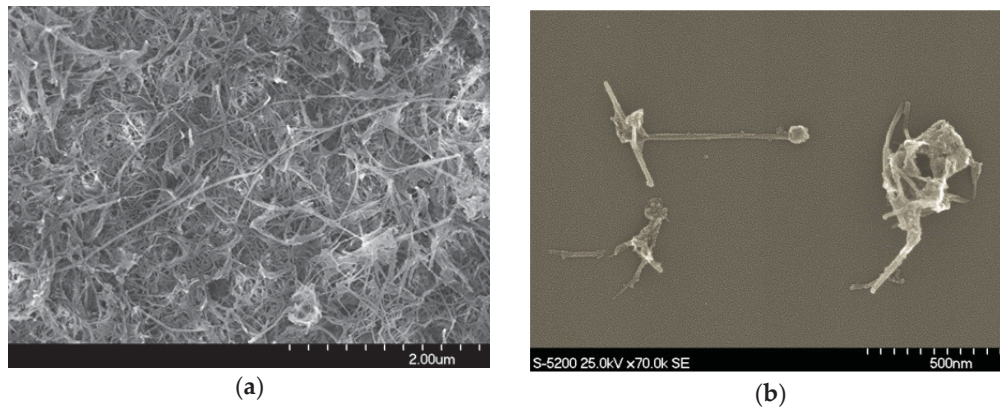
(**a**)   (**b**)

Figure 3. SEM images of (**a**) bulk BNNT material and (**b**) isolated nontube impurities.

Three prototype targets were tested at the RDS-111 cyclotron at Lawrence Berkeley National Laboratory (LBNL) using commercially available BNNT nanomaterials from supplier BNNT, LLC [16]. Preliminary work was performed using BNNT nanomaterials with natural-abundance boron and a target for the Eclipse target changer. The target, shown in Figure 4, features an aluminum target body with a cylindrical target chamber 1.0 cm in diameter by 1.0 cm in length. A window foil of either 25 μm of Havar or 30 μm of aluminum is used to result in a mean incident energy on the BNNT target media of 10.5 MeV or 8.1 MeV, respectively. Annular space between the target and changer creates a flow path for water cooling. Two 1-mm diameter passages, which intercept the target chamber front and rear, allow sweep gas to pass into the target through the BNNT material and out of the target into a delivery line during or after the irradiation process.
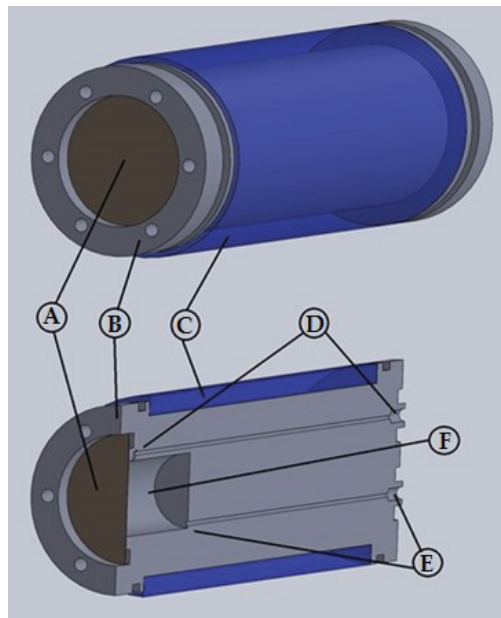

Figure 4. Prototype target for Eclipse target changer including (A) Havar or aluminum window foil, (B) an aluminum target body, (C) cooling water, (D) a front sweep gas flow path, (E) a rear sweep gas flow path, and (F) a target chamber for BNNT.

Using the initial prototype, sufficient quantities of ^{11}C were produced and recovered using a range of operating conditions to demonstrate the feasibility of using BNNT as a target material, and more than 80% of the recovered ^{11}C was in the desired form of CO_2. The principle technical challenge was

identified to be minimizing damage to the BNNT target media that occurred during target operation at a high current. Irradiation at 20 μA with 10.5-MeV incident protons resulted in a dramatic reduction in ^{11}C saturation yield and physical damage to the BNNT material, including the formation of a cavity in the center of the target chamber with translucent glassy crystals along its margins, as shown in Figure 5. The crystalline material was presumed to be boron oxide (B_2O_3).
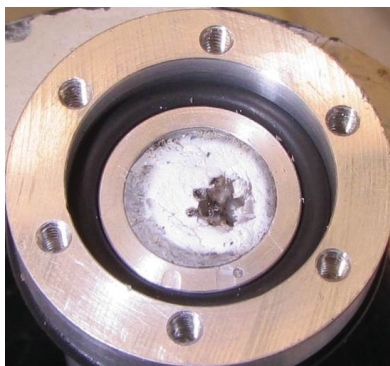

Figure 5. Photograph of BNNT material in the prototype target, showing material damage resulting from irradiation at 20-μA beam current.

Two additional prototype targets with larger chamber volumes were developed for the single target station. The aluminum target bodies feature cylindrical target chambers with dimensions of 1.1 cm in diameter by 6.0 cm in length (BN-124 target) and 1.1 cm in diameter by 1.5 cm in length (BN-131 target), with four 6.1-mm in diameter water cooling channels. Helium-cooled Havar vacuum and target windows (25 μm and 38 μm, respectively) resulted in a mean incident energy on the BNNT media of 9.5 MeV. The BN-124 and BN-131 targets are shown in Figures 6 and 7.
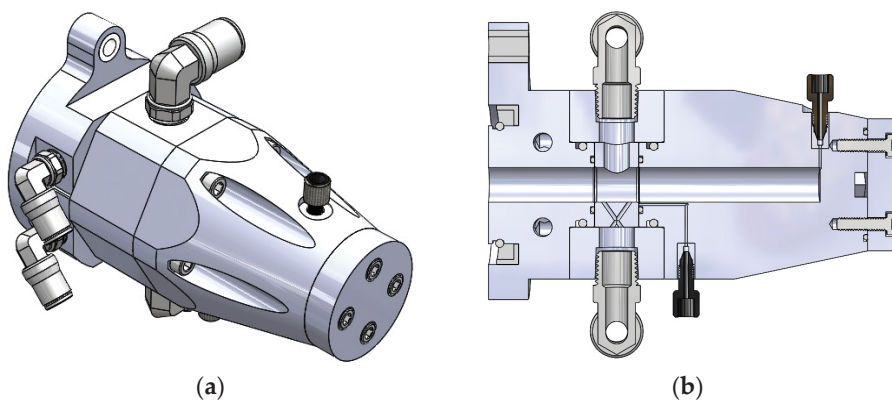

(**a**)   (**b**)

Figure 6. BN-124 target: (**a**) Isometric and (**b**) vertical mid-plane cross-section views.

A custom BTI Targetry target station, shown in Figure 8, was used, consisting of a beam tube, a vacuum isolation valve, a collimator with an 8-mm diameter opening, and target mounting geometry. Because the BN-124 prototype target is considerably longer axially than the prior prototype or commercial ^{18}F targets, the target–collimator interface is subjected to a greater bending moment while supporting the weight of the target. A pressed stainless steel pin on the vertical mid-plane was added to provide additional mechanical support for this application.
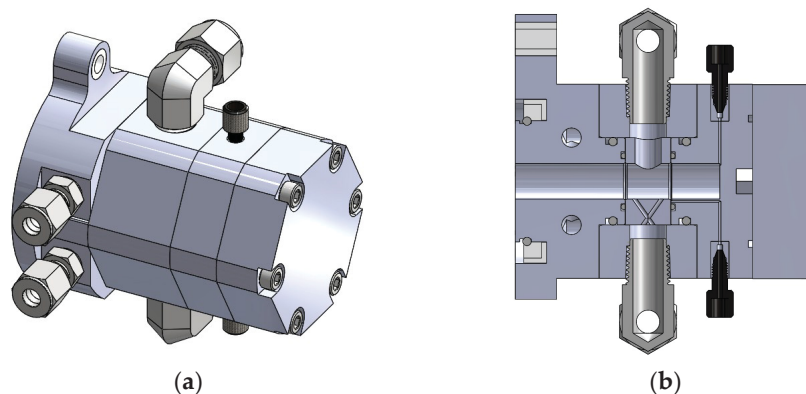
Figure 7. BN-131 target: (**a**) Isometric and (**b**) vertical mid-plane cross-section views.
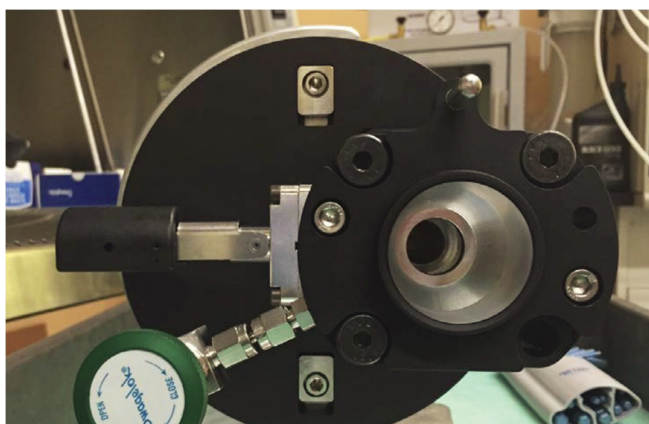

Figure 8. Custom target station with mechanical support for additional axial target depth.

A diagram of the experimental setup is shown in Figure 9. The target chamber was filled with BNNT and pressurized by opening the target isolation valve and delivering gas through a flow control valve. For static mode irradiations, the target load valve was closed, and the target was irradiated at a fixed current. After irradiation, the target unload valve was opened, and the target was allowed to depressurize, followed by opening the load valve to sweep gas through the target chamber and remove volatile radioisotopes. For continuous flow mode irradiations, both the load and unload valves were opened with a gas sweep rate established by the flow control valve, and gas was swept through the target chamber throughout the irradiation. In all cases, the same gas was used to both fill the target and for the sweep to remove volatile radioisotopes. Experiments were performed using a fill gas of nitrogen or helium with 1%–10% oxygen.

For both static and continuous flow operation, the target gas was delivered through 10 m of 0.5-mm inside diameter tubing (valve E to trap G in Figure 9) to a hot cell in the laboratory. Once inside the hot cell, the gas was swept through a $^{11}CO_2$ soda lime trapping cartridge, and the untrapped radiolabeled gases and target gas were collected in a Tedlar gas collection bag. The CO and CO_2 were identified using an SRI 8610C gas chromatograph (GC) equipped with a Restek ShinCarbon ST 80/100 column (P/N 80486-800, 2 m, 2-mm inside diameter, 1/8-in. outside diameter Silicone). The original GC detector setup was a thermal conductivity detector (TCD) followed by a flame ionization detector (FID). A 1/16-in. outside diameter stainless steel line was added in between the two detectors and formed into a 1-in. loop to redirect flow through an NaI gamma detector with outside dimensions roughly 1 in. outside diameter by 4.75 in. high. A Carroll & Ramsey Associate post-amplifier/integrator (model 105-S) was used.
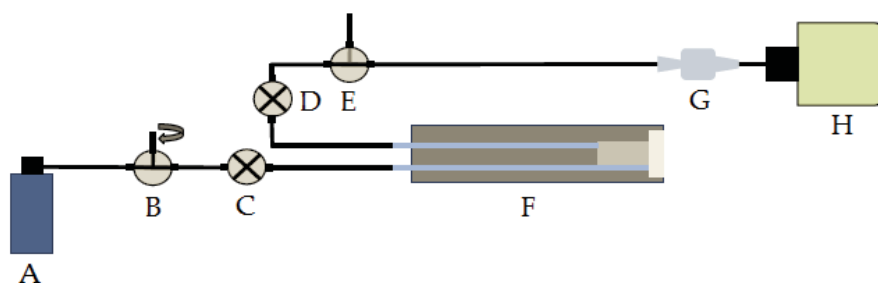
Figure 9. Diagram of experimental apparatus for material irradiation and isotope collection, illustrating a (A) target gas tank and regulator, (B) flow control valve, (C) target load valve, (D) target unload valve, (E) delivery/waste valve, (F) target body and target material, (G) soda lime carbon dioxide trap, and (H) radioisotope gas collection bag.

During the collection, the $^{11}CO_2$ trap was held in a dose calibrator (ionization chamber style well detector) to measure the dynamic buildup and final quantity of ^{11}C trapped as $^{11}CO_2$ on the cartridge. Subsequently, a 50-mL sample of the volatile gases collected in the sampling bag was analyzed for radioactivity in the dose calibrator, and total activity in the bag was determined by volume ratio between the 50-mL sample and total bag volume. Activities of all samples were measured for a minimum of 5 min and fitted to the known half-lives for ^{11}C and ^{13}N, and the results were decay-corrected to end of bombardment.

The ^{11}C was collected in several modes, depending on the experiment (soda lime trap and collection bag, soda lime trap and waste line, or collection bag only). The soda lime trap was made of Fisher Scientific brand (ACS certified, S-196) soda lime placed inside of a Swagelok 1/2–1/4 in. reducing union (PFA-820-6-4) with an approximate volume of 2–4 mL. The collection bag was a 3-L Tedlar bag (SKC Inc., Cat # 232-03). When a GC sample was to be analyzed, the entire target output was collected into the collection bag, and a 1-mL sample was injected onto the GC. Soda lime trap and collection bag mode was used when the CO_2 composition was unknown to determine the percentage of recovered activity in the form of CO_2 versus other radioactive products. Soda lime trap and waste line mode was used to determine target yield when the CO_2 percentage was known to be high.

The recovered target saturation yield of ^{11}C (Y_{sat}) was calculated by

$$Y_{sat} = \frac{A_{EOB}}{I(1 - e^{-\lambda t_{irr}})},$$ (1)

using the recovered decay-corrected end-of-bombardment ^{11}C activity (A_{EOB}), the average beam current (I), the ^{11}C decay constant ($\lambda = 0.034045$ min^{-1}), and a 5-min irradiation time (t_{irr}). A portion of the produced ^{11}C activity remained trapped in the target media but could not easily be measured.

The BN-124 and BN-131 prototype targets were tested using 98% enriched ^{11}B BNNT ($^{11}BNNT$) to increase the yield of ^{11}C and reduce the production of ^7Be, which has a half-life of 53 days. Additional tests were performed for the BN-131 target using $^{11}BNNT$ material from a second commercial supplier, BNNano [18].

3. Results

3.1. Beam Tests of the BN-124 Target

Proton beam tests were performed on the single target station using the BN-124 prototype, which had a 6.0-cm depth and a 5.7-cm^3 volume, for beam currents between 1 and 10 μA, with static operation at load pressures between 200 and 800 psi using a fill gas of nitrogen with 1% oxygen. The target was loaded with 377 mg of $^{11}BNNT$, corresponding to an effective BNNT density of 0.07 g/cm^3. A recovered target saturation yield of $^{11}CO_2$ as a function of beam current and load pressure is shown

in Figure 10. More than 95% of the recovered activity was in the desired form of $^{11}CO_2$, as indicated by soda lime trapping and confirmed by GC measurements. Target saturation yield increased with pressure between 200 and 600 psi, and then began to drop off. Saturation yield was highest at 1 μA, which corresponded to the lowest target heat input.
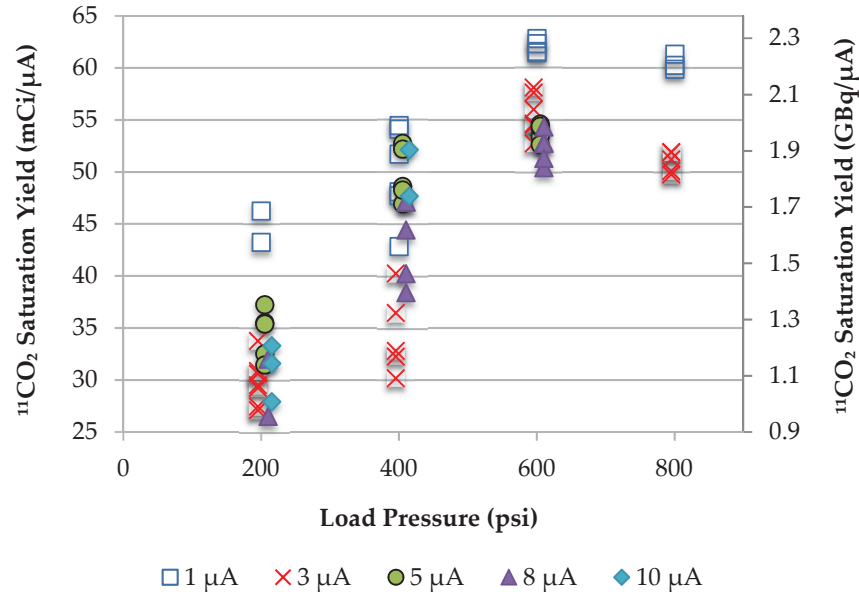

Figure 10. $^{11}CO_2$ saturation yield for the BN-124 target using a fill gas of nitrogen with 1% oxygen.

The BN-124 target was opened and visually inspected following a series of irradiations at each beam current. Following irradiation at 1 μA, the material changed color from gray to off-white, which was attributed to the conversion of elemental B impurities into B_2O_3. Material shrinkage (volume reduction) of the BNNT target media into the back of the target was observed, with additional shrinkage occurring for higher currents, as summarized in Table 1. After irradiation at 3 μA, the material shrinkage was about 40%, and the color continued to whiten. Following the 8-μA runs, observed changes in the BNNT material included crystallization, gray and black spots, and a white powdery buildup coating the inside walls of the target. Due to the additional material shrinkage, there was a 3.1-cm depth void in the front of the target, which was more than half of the chamber depth.

Table 1. Material shrinkage measurements and visual observations for the BN-124 target.

Beam Current (μA)	Depth of Void (cm)	Depth of $^{11}BNNT$ (cm)	Observations
0	-	6.0	Gray color
1	-	6.0	Off-white color
3	2.5	3.5	White color, shrinkage
5	2.5	3.5	White color, shrinkage
8	3.1	2.9	Crystallization, powdery buildup coating walls

Photographs of the BN-124 target media post-irradiation at each beam current are shown in Figure 11. It is important to note that shades of gray and white can be very misleading due to variations in the angle of the photograph and lighting conditions.
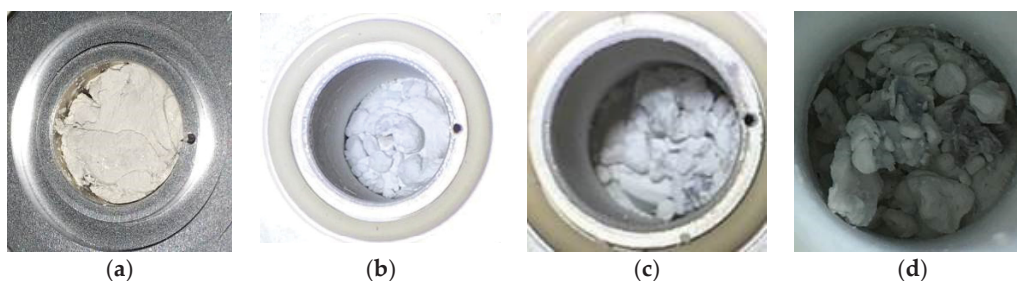
Figure 11. Photographs of the BN-124 target post-irradiation at (**a**) 1 μA; (**b**) 3 μA; (**c**) 5 μA; and (**d**) 8 μA.

The void formed in the front of the target during irradiation made interpretation of the data difficult, since most of the recovered yield was likely from the $^{14}N(p,\alpha)^{11}C$ reaction in the nitrogen gas in the voided region. Increasing the effective density in the BN-124 target to mitigate material shrinkage would have required significantly more $^{11}BNNT$ material, which was both cost-prohibitive (>$1000/g) and inefficient due to the range of the protons. Accounting for the Havar vacuum and target windows (25 μm and 38 μm, respectively), stopping power calculations indicated only 125 mg of BNNT was needed for the target to be axially range thick for 11-MeV protons.

3.2. Beam Tests of the BN-131 Target

To address these issues, a second prototype target (BN-131) was designed and fabricated for the single target station with a reduced target depth of 1.5 cm, resulting in a volume of 1.4 cm^3. The target was loaded with 400 mg of $^{11}BNNT$, resulting in an effective BNNT density four times higher than that used for the prior prototype. Proton beam irradiations were performed at 5 μA, for static operation at 200–600 psi load pressure, using both nitrogen gas with 1% oxygen and helium gas with 1% oxygen. Negligible material shrinkage was observed for the BN-131 target following irradiation.

Total saturation yield of ^{11}C in all forms ($^{11}CO_2$ and ^{11}CO) for the BN-131 target irradiations is shown in Figure 12. Since helium does not offer a competing production reaction for ^{11}C, all recovered ^{11}C was produced in BNNT for these irradiations. The total yield of ^{11}C was roughly equivalent for both gases, suggesting minimal production of ^{11}C in the nitrogen fill gas. The fraction of activity recovered in the form of carbon dioxide is shown in Figure 13. Using helium fill gas in the BN-131 target consistently produced less ^{11}C as CO$_2$ (35%–55%) compared to using nitrogen gas in the BN-131 target (50%–55%). For both fill gases, the percentage of activity recovered as carbon dioxide was significantly less than that observed when using nitrogen gas in the BN-124 target (>95%).
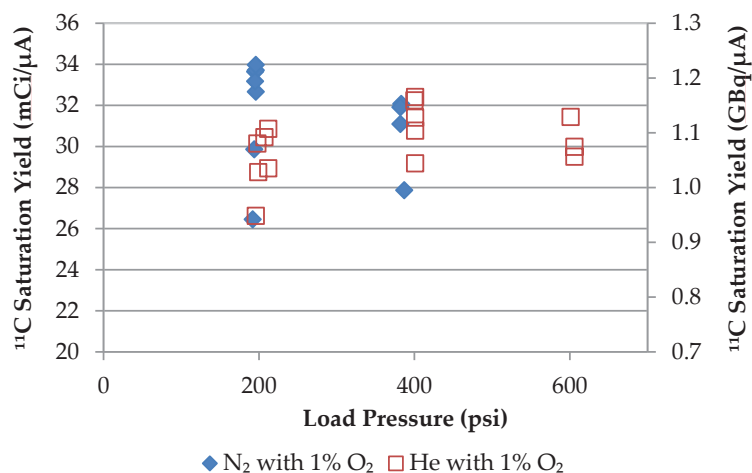

Figure 12. ^{11}C saturation yield for the BN-131 target at 5 μA.
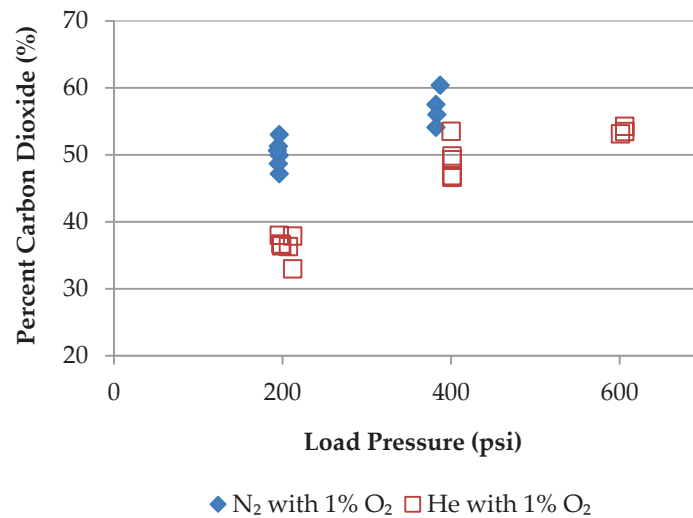
Figure 13. Percent of ^{11}C recovered as CO_2 for the BN-131 target at 5 μA.

3.3. Comparison of ^{11}C Saturation Yield for the BN-124 and BN-131 Targets

Total saturation yield of ^{11}C in all forms ($^{11}CO_2$ and ^{11}CO) for the BN-124 and BN-131 targets is shown in Figure 14. The results were similar for static operation using a fill gas of nitrogen with 1% oxygen at 200 psi. However, the BN-124 target yield increased with nitrogen gas pressure, while the BN-131 target yield was insensitive to nitrogen gas pressure. This supported the assertion that a significant component of yield from the larger target was due to ^{11}C production in the voided region and independent of the nanomaterials.
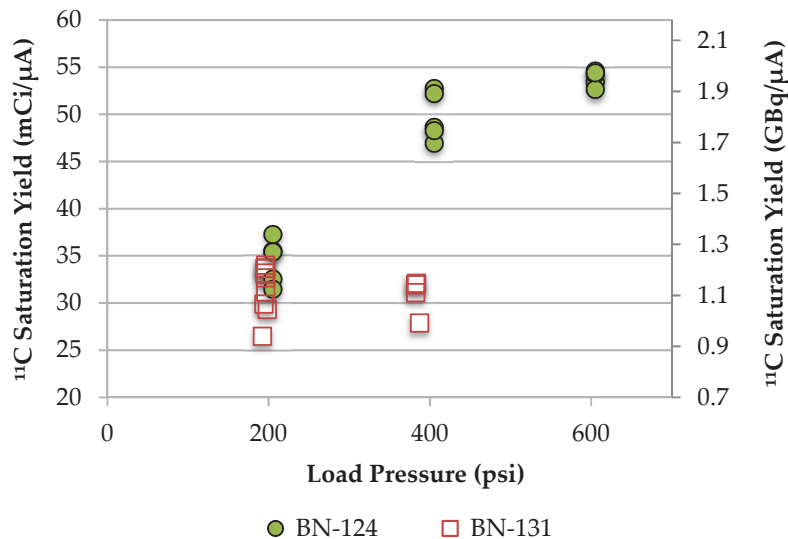

Figure 14. ^{11}C saturation yield for the BN-124 and BN-131 targets at 5 μA using nitrogen with 1% oxygen.

3.4. BN-124 Gas-Only Target Operation

To provide a better context for evaluating target performance, the BN-124 target was also operated as a gas target using a fill gas of nitrogen with 1% oxygen with no BNNT nanomaterials present. The recovered target saturation yield of $^{11}CO_2$ for static operation at 200 psi load pressure using 377 mg ^{11}BNNT and for gas-only static operation at 200 psi load pressure is shown in Figure 15. Monte Carlo radiation transport calculations were performed for the target using Monte Carlo N-Particle eXtended

(MCNPX) [19]. Although MCNPX simulations using the nuclear cross-section data indicated more ^{11}C was produced when using the [11]BNNT, use of the [11]BNNT resulted in a lower recovered saturation yield for all cases. This suggested a large amount of activity was being trapped in the target.
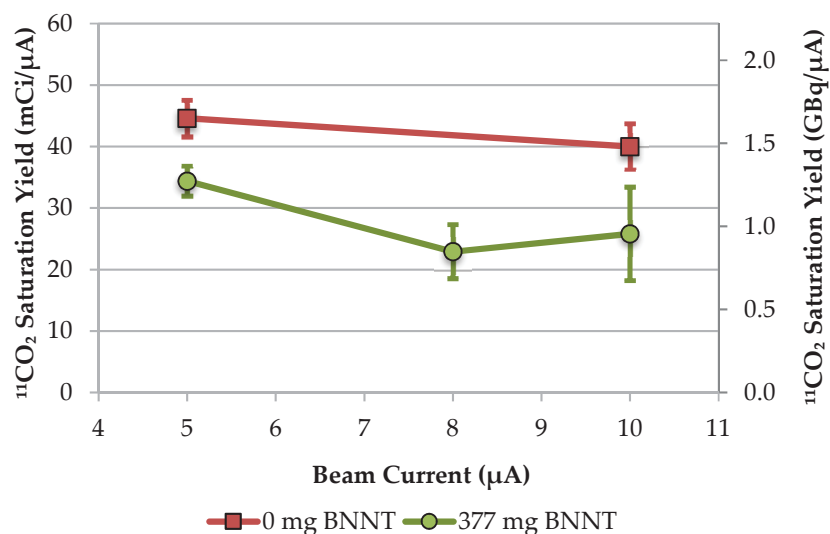

Figure 15. [11]CO_2 saturation yield for the BN-124 target using a fill gas of nitrogen with 1% oxygen.

3.5. Evaluation of BNNT Nanomaterials from a Second Supplier

Additional BNNT nanomaterials were acquired from a second manufacturer, BNNano [18]. Low-purity material (<90% nanotubes) was selected to prevent the material from becoming too brittle to easily load in the cylindrical target chamber. The material was darker in color, with significantly higher density and more mechanical integrity when manipulated, although it was still susceptible to plastic deformation. Photographs of bulk BNNT material from the two suppliers are shown in Figure 16. A limited set of ^{11}C saturation yield data was collected using the BN-131 target with [11]BNNT nanomaterials from BNNano at the RDS-111 cyclotron at LBNL and at a commercial RDS-111 cyclotron operated by Triad Isotopes. The saturation yield data were 1–2 orders of magnitude lower than what was observed in the prior tests using [11]BNNT from BNNT, LLC. SEM imaging revealed a much higher concentration of nontube impurities in the material, as shown in Figure 17. This further supported the theory that high-purity material was needed to prevent ^{11}C trapping in targets and achieve a high recovered saturation yield.
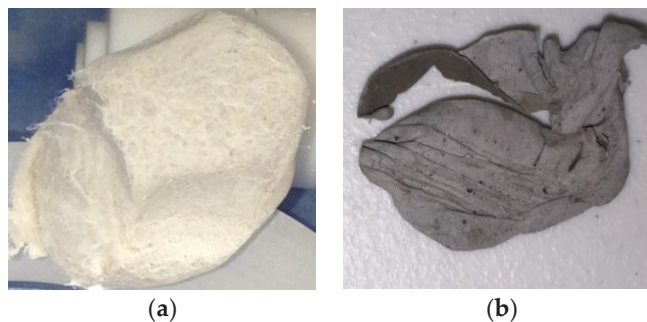

(**a**)   (**b**)

Figure 16. Photographs of BNNT nanomaterials from (**a**) BNNT, LLC, and (**b**) BNNano.
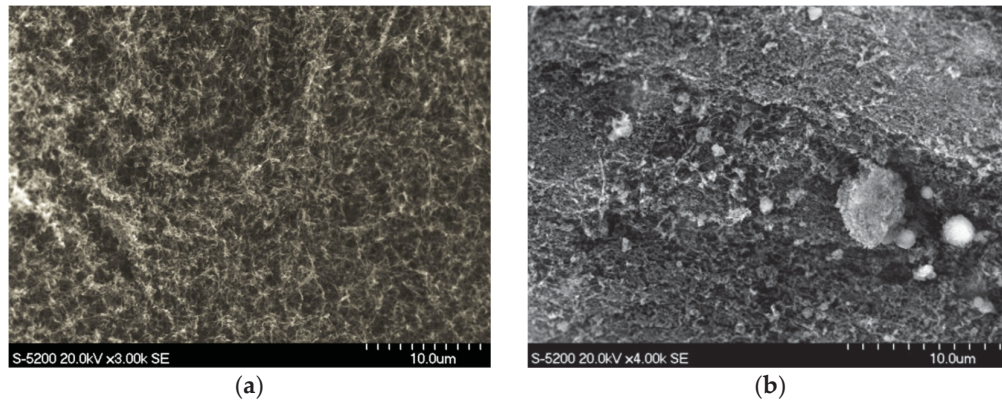
(**a**)   (**b**)

Figure 17. SEM images of BNNT nanomaterials from (**a**) BNNT, LLC, and (**b**) BNNano.

4. Discussion

Use of BNNT nanomaterials in a recoil escape target has the potential to increase ^{11}C yield for proton energies at or below 11 MeV by utilizing both the ^{11}B(p,n)^{11}C and ^{14}N(p,α)^{11}C nuclear reactions. However, additional studies are needed to determine operating conditions suitable for a commercial product. Beam irradiation experiments at a low effective BNNT density resulted in material shrinkage, making interpretation of the data difficult. Operating at a higher effective BNNT density prevented material shrinkage, but resulted in a lower saturation yield of ^{11}C and a lower percentage of activity recovered in the desired form of CO_2.

Poor recovery of produced ^{11}C and material degradation at modest beam currents both pose significant challenges for the development of a commercial system. The trapping of produced ^{11}C in the target was most likely a function of the nontube impurities present in the commercially sourced BNNT nanomaterials. Impurities could be removed prior to irradiation by thermal oxidation in a furnace, followed by a water rinse. Future work will include beam irradiation tests of a sample of ^{11}BNNT that has been purified at 600 °C for 1 h at the National Institute of Aerospace (NIA). ^{11}BNNT material as-received from the BNNT, LLC, supplier is shown next to the purified material (which is layered with wax paper) in Figure 18. The purified material is whiter in color, more brittle, and has increased density of roughly one order of magnitude.

Figure 18. Photograph of 500-mg sample of as-received BNNT (left) and 500-mg sample of BNNT following purification at the National Institute of Aerospace (NIA) at 600 °C for 1 h (right).

Material degradation of BNNT materials has been observed as a function of beam current, due to elevated temperature in the target. Bulk BNNT material has low effective thermal conductivity of roughly 1 W/m^2-K [20], and significant thermal oxidation has been observed for BNNT targets in the range of 800–900 °C [21]. A new target prototype is currently being designed that aims to reduce peak temperature in the BNNT by utilizing a grazing angle for the beam with only a thin layer of BNNT.

The grazing angle prototype target will use high-purity BNNT target media (99% nanotubes and 1% nontube impurities of B and *h*-BN) from supplier BNNano.

References

1. Rubio, A.; Corkill, J.L.; Cohen, M.L. Theory of graphitic boron nitride nanotubes. *Phys. Rev. B* **1994**, *49*, 5081–5084. [CrossRef]
2. Weng-Sieh, Z.; Cherrey, K.; Chopra, N.G.; Blase, X.; Miyamoto, Y.; Rubio, A.; Cohen, M.L.; Louie, S.G.; Zettl, A.; Gronsky, R. Synthesis of $B_xC_yN_x$ nanotubules. *Phys. Rev. B* **1995**, *51*, 11229–11232. [CrossRef]
3. Chopra, N.G.; Luyken, R.J.; Cherrey, K.; Crespi, V.H.; Cohen, M.L.; Louie, S.G.; Zettl, A. Boron nitride nanotubes. *Science* **1995**, *269*, 966–967. [CrossRef] [PubMed]
4. Smith, M.W.; Jordan, K.C.; Park, C.; Kim, J.W.; Lillehei, P.T.; Crooks, R.; Harrison, J.S. Very long single- and few-walled boron nitride nanotubes (BNNTs) via the pressurized vapor/condenser method. *Nanotechnology* **2009**, *20*, 505604. [CrossRef] [PubMed]
5. Kim, K.S.; Kim, M.J.; Park, C.; Fay, C.C.; Chu, S.H.; Kingston, C.T.; Simard, B. Scalable manufacturing of boron nitride nanotubes and their assemblies: A review. *Semicond. Sci. Technol.* **2016**, *32*, 013003. [CrossRef]
6. Jensen, M.; Eriksson, T.; Severin, G.; Parnaste, M.; Norling, J. Experimental yields of PET radioisotopes from a prototype 7.8 MeV cyclotron. In Proceedings of the 15th International Workshop on Targetry and Target Chemistry, Prague, Czech Republic, 18–21 August 2014; pp. 112–113.
7. Khachaturian, M.; Bailey, J. The ABT Molecular Imaging biomarker generator Dose-on-Demand™ high flow tantalum 1.0 water target. In Proceedings of the 16th International Workshop on Targetry and Target Chemistry, Santa Fe, NM, USA, 29 August–1 September 2016; pp. 2–4.
8. Smirnov, V.; Vorozhtsov, S.; Vincent, J. Design study of an ultra-compact superconducting cyclotron for isotope production. *Nucl. Instr. Meth. Phys. Res. A* **2014**, *763*, 6–12. [CrossRef]
9. Podadera, I.; Ahedo, B.; Arce, P.; García-Tabarés, L.; Gavela, D.; Guirao, A.; Lagares, J.I.; Martínez, L.M.; Obradors-Campos, D.; Oliver, C.; et al. Beam diagnostics for commissioning and operation of a novel compact cyclotron for radioisotope production. In Proceedings of the International Beam Instrumentation Conference (IBIC2013), Oxford, UK, 16–19 September 2013; pp. 660–663.
10. Koziorowski, J.; Larsen, P.; Gillings, N. A quartz-lined carbon-11 target: Striving for increased yield and specific activity. *Nucl. Med. Biol.* **2010**, *37*, 943–948. [CrossRef] [PubMed]
11. Savio, E.; García, O.; Trindade, V.; Buccino, P.; Giglio, J.; Balter, H.; Engler, H. Improving production of ^{11}C to achieve high specific labelled radiopharmaceuticals. *AIP Conf. Proc.* **2012**, *1509*, 185–189. [CrossRef]
12. Fonslet, J.; Itsenko, O.; Koziorowski, J. Indirect measurement of specific activity of $[^{11}C]CO_2$ and the effects of target volume fractionation. *AIP Conf. Proc.* **2012**, *1509*, 190–193. [CrossRef]
13. Peeples, J.L.; Magerl, M.; O'Brien, E.M.; Doster, J.M.; Bolotnov, I.A.; Wieland, B.W.; Stokely, M.H. High current C-11 gas target design and optimization using multi-physics coupling. *AIP Conf. Proc.* **2017**, *1845*, 020016. [CrossRef]
14. Firouzbakht, M.L.; Schlyer, D.J.; Wolf, A.P. Yield measurements for the ^{11}B(p,n)^{11}C and ^{10}B(d,n)^{11}C nuclear reactions. *Nucl. Med. Biol.* **1998**, *25*, 161–164. [CrossRef]
15. Takacs, S.; Tarkanyi, F.; Hermanne, A.; Paviotti de Corcuera, R. Validation and upgrade of the recommended cross section data of charged particle reactions used for production PET radioisotopes. *Nucl. Instrum. Methods Phys. Res. B* **2003**, *211*, 169. [CrossRef]
16. BNNT, LLC [US]. Available online: https://www.bnnt.com/products (accessed on 17 December 2018).
17. Zhi, C.; Bando, Y.; Tang, C.; Golberg, D. Specific heat capacity and density of multi-walled boron nitride nanotubes by chemical vapor deposition. *Solid State Commun.* **2012**, *151*, 183–186. [CrossRef]
18. BNNano. Available online: https://www.bnnano.com/products (accessed on 17 December 2018).

19. Pelowitz, D.B. (Ed.) *MCNPX User's Manual Version 2.7.0*; LA-CP-11-00438; Los Alamos National Laboratory: Santa Fe, NM, USA, 2011.

20. Jakubinek, M.B.; Niven, J.F.; Johnson, M.B.; Ashrafi, B.; Kim, K.S.; Simard, B.; White, M.A. Thermal conductivity of bulk boron nitride nanotube sheets and their epoxy-impregnated composites. *Phys. Status Solidi A* **2016**, *213*, 2237–2242. [CrossRef]

21. Chen, Y.; Zou, J.; Campbell, S.J.; Le Caer, G. Boron nitride nanotubes: Pronounced resistance to oxidation. *Appl. Phys. Lett.* **2004**, *84*, 2430. [CrossRef]